Molecular Crystals and Liquid Crystals

ISSN: 1542-1406 (Print) 1563-5287 (Online) Journal homepage: http://www.tandfonline.com/loi/gmcl20

Discovery of Liquid Crystal Mesophases with a Six-Layer Periodicity

C. C. Huang, Shun Wang, Lidong Pan, P. Barois & Ron Pindak

To cite this article: C. C. Huang, Shun Wang, Lidong Pan, P. Barois & Ron Pindak (2015) Discovery of Liquid Crystal Mesophases with a Six-Layer Periodicity, Molecular Crystals and Liquid Crystals, 610:1, 23-34, DOI: 10.1080/15421406.2015.1025200

To link to this article: http://dx.doi.org/10.1080/15421406.2015.1025200

Mol. Cryst. Liq. Cryst., Vol. 610: pp. 23–34, 2015

ISSN: 1542-1406 print/1563-5287 online
DOI: 10.1080/15421406.2015.1025200

Discovery of Liquid Crystal Mesophases with a Six-Layer Periodicity

C. C. HUANG,[1,*] SHUN WANG,[2] LIDONG PAN,[1,3] P. BAROIS,[4] AND RON PINDAK[5]

[1]School of Physics and Astronomy, University of Minnesota, Minneapolis, MN, USA
[2]Department of Physics and Astronomy, Key Laboratory of Artificial Structures and Quantum Control (Ministry of Education), Shanghai Jiao Tong University, Shanghai, China
[3]Department of Physics and Astronomy, Johns Hopkins University, Baltimore, MA, USA
[4]University of Bordeaux, CNRS, CRPP, Pessac, France
[5]Photon Sciences Directorate, Brookhaven National Laboratory, Upton, NY, USA

*In 2006, employing ellipsometry and resonant x-ray diffraction, our research group discovered a liquid crystal mesophase having a six-layer periodicity in a ternary mixture (*mixture A*) as well as in a binary mixture (*mixture B*). This phase shows antiferroelectric-like properties. Subsequently, J. K. Vij's group used field-induced birefringence to explore the physical properties of various binary mixtures similar to* mixture B. *Recently, Y. Takanishi* et al. *obtained dielectric responses and two-dimensional microbeam resonant x-ray diffraction profiles as a function of temperature from a different binary mixture with one compound of the mixture containing a central bromine atom. They discovered another new mesophase which shows a six-layer structure and displays ferrielectric-like responses along with a different phase sequence. This article will review the sequence of events leading up to the discovery of the new phases with a six-layer periodicity and highlight differences in conclusions about the new phases and an ongoing debate about the existence of a phase with five-layer periodicity.*

Keywords $SmC_{d6}{}^{*}$ phase, resonant x-ray diffraction, null transmission ellipsometry, SmC^{*} variant phases

Introduction

Smectic liquid crystals consist of elongated semi-flexible organic molecules arranged in layer structures. Within each layer, molecules possess a liquid-like arrangement [1, 2]. The director $\tilde{n}_j$ specifies the molecular long axis in the j-th layer. The projection of $\tilde{n}_j$ on the layer plane is defined as the vector $\mathbf{c_j}$. $\tilde{n}$ and $\mathbf{c}$ may vary from layer to layer, yielding various smectic phases. In the smectic-A (SmA) phase, the director $\tilde{n}$ is parallel to the layer normal

*Address correspondence to C. C. Huang, School of Physics and Astronomy, University of Minnesota, Minneapolis, MN 55455, USA. E-mail: cchuang@gmail.com

Color versions of one or more of the figures in the article can be found online at www.tandfonline.com/gmcl.

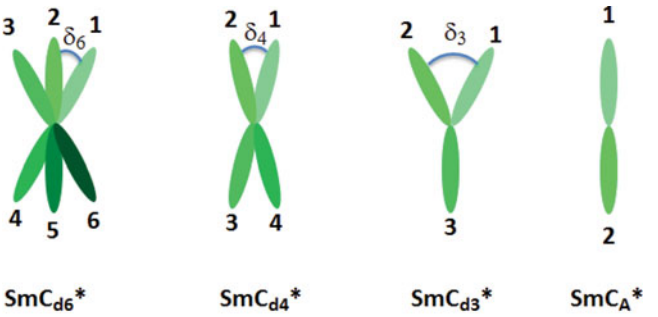

Figure 1. The molecular arrangements of four SmC* variant phases: SmC_{d6}*, SmC_{d4}*, SmC_{d3}*, and SmC_A*. There are optical pitches superimposed on these nano-scale structures. For clarity, different notations have been assigned to the distortion angles (δ's) for different phases.

(**z**), while in the smectic-C (SmC) phase, $\tilde{n}$ tilts at a finite angle from the **z**-axis. For chiral liquid crystal compounds, the azimuthal orientation of $\tilde{n}$ usually varies from layer to layer. Thus, various chiral smectic-C (SmC*) phases have been found.

Antiferroelectric liquid crystals (AFLC) present an interesting class of materials that show many different SmC* phases, namely, SmC* variant phases. At a given temperature, the magnitude of tilt angle is constant through-out the bulk sample, while the azimuthal angles change in different layers. Before our experimental discovery of the SmC_{d6}* (the SmC* variant phase with a six-layer periodicity and a distorted (subscript-d) helical structure) five distinct SmC* variant phases were well-characterized. They are SmC_α*, SmC*, SmC_{d4}*, SmC_{d3}*, and SmC_A* [3]. Here SmC_α*and SmC* display a uniform helical formation with a short (roughly less than 10 layers) and long (approximately 100 layers) pitch, respectively. The SmC_{d4}* (SmC_{d3}*) shows a 4- (3-) layer distorted helical structure characterized by different distortion angles δ's. See Fig. 1. Previously, the naming convention of SmC_β*, SmC_{FI2}*, $SmC_{1/4}$*, or SmC_A*($q_T = 1/2$) has been used by various groups for the SmC_{d4}* phase while SmC_γ*, SmC_{FI1}*, $SmC_{1/3}$*, or SmC_A*($q_T = 1/3$) has been used for the SmC_{d3}* phase. Finally, the SmC_A* is a 2-layer antiferroelectric phase. In addition to the short periodicities characterizing SmC_{d4}*, SmC_{d3}*, and SmC_A* phases, usually a μm-scale (optical) helical pitch is superimposed.

Out of several hundred AFLC compounds that have been studied, almost all of them showed the following phase sequence: SmA- SmC_α*-SmC*-SmC_{d4}*-SmC_{d3}*-SmC_A* upon cooling. Some of these phases may be missing in most compounds. Employing optical studies on a homologous series of benzoate ester compounds (nOHFBBB1M7 (nOHF)), V. Laux *et al*. [4] reported an unusual phase sequence of 10OHF upon cooling, namely, SmA- SmC_α*- SmC_{FI}*- SmC*. Employing optical and resonant x-ray diffraction (RXRD), six years later S. T. Wang *et al*. confirmed this phase sequence reversal behavior in the pure 10OHF (with the identification of the SmC_{FI}* to be SmC_{d4}*) and the binary mixtures of 10OHF and 9OTBBB1M7 (C9) [5]. The homologous mesogens nOTBBB1M7 (Cn) which contain a sulfur atom in the core part of the molecule are the key compounds for our RXRD studies utilizing the K_α absorption edge (at 2. 471 *KeV*) of the sulfur atom. Adding C9 to 10OHF not only allows us to conduct RXRD experiments but also significantly increases the temperature range of the SmC_{d4}* phase. Through extrapolation, the RXRD results enable us to conclude that our ellipsometric data from pure 10OHF definitely display the SmC_α*-SmC_{d4}*- SmC* phase reversal behavior. Later, K. L. Sandhya *et al*. [6] obtained results from

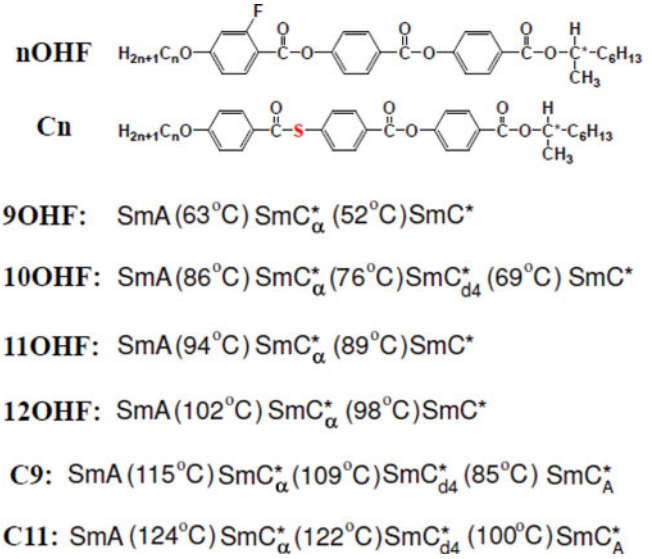

Figure 2. The chemical structures and phase sequences (upon cooling) of the homologous series nOHF and Cn. The sulfur atoms in the Cn compounds are essential for the RXRD experiments.

optical birefringence, spontaneous polarization, selective reflection, conoscopy, along with dielectric spectroscopy. The reported phase reversal behavior of 10OHF was confirmed. They also reported hysteresis of the phase sequence. Namely, upon cooling pure 10OHF exhibits the SmC_α^*- SmC_{d4}^*- SmC^* phase while heating from the SmC^* phase, it changes to the SmC_α^* phase without the SmC_{d4}^* phase. Such a thermal hysteresis disappears in the mixture with a small amount of C9. Chemical structures and transition temperatures of several relevant nOHF and Cn compounds are given in Fig. 2.

Ordinary x-ray diffraction (XRD) which probes the scalar scattering structural factor can only yield the smectic layer structure. In contrast, resonant XRD (RXRD), which is sensitive to the tensorial scattering structural factor from the sample, can provide additional information relating to the orientational order [7, 8]. To date, RXRD remains the most powerful and direct experimental probe to characterize the molecular structures of various SmC^* variant phases or identify a new mesophase showing a different orientational order. Thus far, compounds containing sulfur, selenium or bromine [8-11] in the core part of molecules have been used extensively in pure compounds or mixtures with other compounds for the RXRD studies. In reality besides the distinct nano-scale structures characterizing the SmC_{d4}^*, SmC_{d3}^*, and SmC_A^* phases, they also show long helical pitches. This additional large-length structure yields split RXRD satellite peaks which enables us to obtain magnitudes of both distortion angles (δ) and the optical helical pitch [12].

Discovery of SmC_{d6}^* Phase

Among members of the nOHF homologous series, only 10OHF shows the distinctive SmC_α^*- SmC_{d4}^*- SmC^* phase reversal phenomenon [4, 13]. By adding a sufficient amount of either 9OHF (about 50%) or 11OHF (about 25 %) to 10OHF, the phase reversal phenomena are totally suppressed [13]. The fact that adding C9 to 10OHF enhanced the

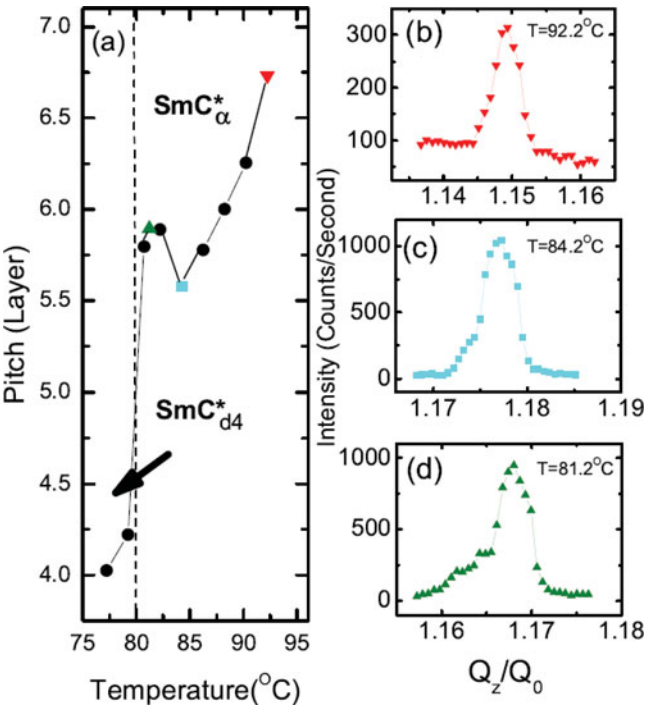

Figure 3. (a) The pitch temperature evolution of the "first batch" *mixture A* in the SmC_α^* phase measured by RXRD. (b)-(d) X-ray scan data of the mixture at 92.2°C, 84.2°C and 81.2°C. The abrupt increase in pitch upon cooling provided us an important hint of the existence of a new mesophase.

temperature window of the SmC_{d4}^* phase led us to prepare several ternary mixtures. In the binary mixture $(10OHF)_{0.73}$-$(11OHF)_{0.27,}$ the SmC_{d4}^* phase becomes undetectable from our ellipsometric data [13]. As anticipated, the phase reversal behavior is recovered by adding C9 (only 15%) to this binary mixture in our RXRD studies. For convenience of our discussion, this ternary mixture ($(73\%\ 10OHF/\ 27\%11OHF)_{0.85}\ C9_{0.15}$) will be called *mixture A*. Our preliminary RXRD results from *mixture A* not only confirm the reappearance of the phase reversal behavior but also exhibit an intriguing hump (with pitch $\approx$ 6 layers) between the SmC_α^* and SmC_{d4}^* phases in the pitch vs. temperature plot [13]. See Fig. 3.

Soon afterward, our in-house ellipsometric studies revealed an antiferroelectric-like response in this region of the hump. Figure 4 shows a temperature variation plot of one of the ellipsometric parameters (Δ) with two different orientations of applied electric field to a free standing film of *mixture A* having thickness $\approx$80 layers. Such free-standing liquid crystal films will have net polarization. Thus an external applied electric field can be utilized to place the whole films in a specific orientation while film optical properties are acquired. This set of specific anti-parallel electric field orientations are chosen to bring out the maximum information related to the molecular arrangements in the free standing films. Above T_1, the split between Δ_{90} and Δ_{270} indicates a surface-induced synclinic arrangement in the bulk SmA-temperature window. This is a manifestation of the surface-induced order commonly found near most air-liquid crystal interfaces. Upon cooling, the oscillations of the Δ's found between T_1 and T_2 imply a temperature evolution of the short-helical pitch and are a signature of the SmC_α^* phase [14, 15]. Another evident feature is distinct jumps

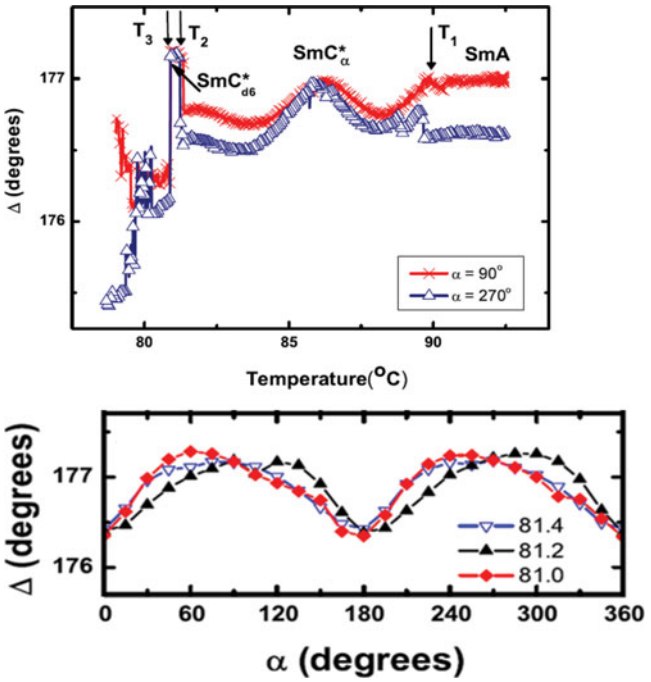

Figure 4. (a) Temperature variation of one of the ellipsometric parameters (Δ) obtained from an 80-layer free-standing film of *mixture A*.The data were acquired under two different applied electric orientations. (b) The ellipsometric parameter (Δ) *vs* the applied electric field orientations (α). The data were obtained in three different temperatures within the $SmC_{d6}{}^*$ temperature window. The 180°-symmetry of the Δ *vs* α indicates antiferroelectric property of this phase.

in Δ at both T_2 and T_3. In the region between these jumps, the fact that the values of Δ_{90} and Δ_{270} are approximately the same signifies an antiferroelectric-like structure. To be sure of an antiferroelectric-like response in the region between T_2 and T_3, we measured the ellipsometric parameter (Δ) as a function of the applied electric field orientation (α). The results from three temperatures yield an approximately 180°-symmetry as shown in Fig. 4.

One year later, our RXRD investigation from thick free-standing films (thickness > 500 layers) of *mixture A* revealed the novel $SmC_{d6}{}^*$ phase with a six-layer periodicity [16]. The data are summarized in Fig. 5. Temperature dependence of both layer spacing (from the principal Bragg-peak positions) and pitch (from the satellite-peak positions) are shown. All our high-resolution x-ray data from principal Bragg peaks are very sharp which indicates that the magnitude of tilt angle is the same within our thick films. Upon cooling from the SmA phase, except a noticeable step-down in the vicinity of the $SmC_\alpha{}^*$- $SmC_{d6}{}^*$ transition and a step-up just below 79°C, the layer spacing (d) decreases monotonically with temperature which is the result of the increase in tilt angle. Meanwhile, the pitch decreases almost linearly from 6.49 to 5.39 layers in the $SmC_\alpha{}^*$ phase. At T = 81.43°C, the pitch shows an abrupt jump to 6.00 layers. This transition is accompanied by a sudden decrease in the layer spacing. The lock-in of the pitch at 6.00 layers over a finite temperature window (approximately 1 K) is a clear signature of the existence of the $SmC_{d6}{}^*$ phase. The jumps indicate that the $SmC_{d6}{}^*$ and $SmC_\alpha{}^*$ are two different phases and the transition between them is first order. Below 81.4°C, layer spacing data decrease slowly which indicates the tilt

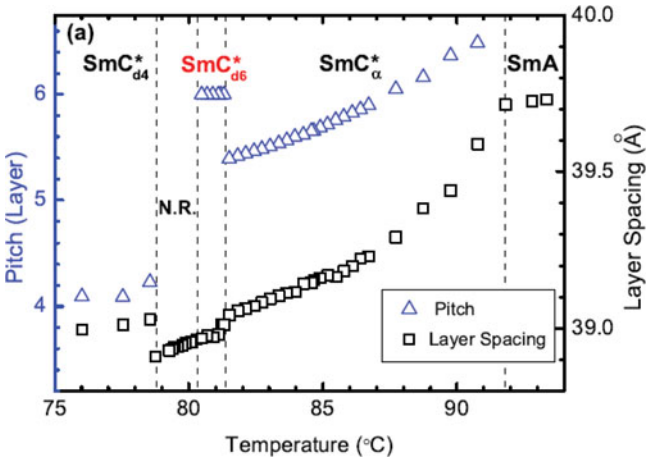

Figure 5. Temperature dependences of pitch (triangles) and layer spacing (squares) for *mixture A*. Different phases are separated by dashed lines. Noisy resonant signals (See Fig. 7) are obtained in the regions between the SmC_{d6}^* and SmC_{d4}^* phases. They are called noisy region (N.R.). No pitch data are given in these regions.

angle almost saturated around the SmC_{d6}^* phase. The temperature evolution of pitch shows one remarkable feature. Upon cooling, it decreases smoothly through six layers within the SmC_{α}^* phase and then jumps to six at a lower temperature. Consequently, there are two structures with a pitch value of a six-layer periodicity in this mixture; (a) a uniaxial SmC_{α}^* structure with a pitch value of six existing at a temperature near $T = 87.72^{\circ}C$ and (b) a biaxial SmC_{d6}^* structure over a temperature range of about 1K. These two structures show very different resonant peaks. Distinctively, the high temperature one has a single satellite peak while the low temperature one shows one set of split satellite peaks.

Before the satellite peaks evolve to Q_z-positions indicative of the 4-layer periodicity of the SmC_{d4}^* phase, between 80.2°C and 78.9°C, there exists a noisy region (N.R.) with featureless and irreproducible RXRD signals over a wide range of Q_z-values (the magnitude of the scattering wave vector). Meanwhile, the shapes of the non-resonant principal peaks remain very sharp. The resonant satellite peaks become sharp again in the SmC_{d4}^* phase; the transition is accompanied by an increase in the layer spacing. Such unique phenomena demonstrate that during the transition from the SmC_{d6}^* to SmC_{d4}^* phase, the layer structure remains well established but the orientation order undergoes complex changes. We will return to this unique behavior in the latter part of the paper. During a subsequent heating cycle, the films showed the SmC_{d6}^* phase before entering the SmC_{α}^* phase. After reviewing the "old" RXRD data, quickly the existence of the SmC_{d6}^* phase in a binary mixture, $(10OHF)_{0.89}$ $(C11)_{0.11}$, (*mixture B*) was confirmed during the same synchrotron run. Again this mixture shows the same phase sequence: SmA- SmC_{α}^*-SmC_{d6}^*-N.R.- SmC_{d4}^* upon cooling.

Figure 6 displays a typical plot of x-ray intensity versus Q_z obtained within the SmC_{d6}^* phase at $T = 80.89^{\circ}C$ of *mixture A*. The data show split resonant peaks centered at $Q_z/Q_o = 1.167$ which indicates that the SmC_{d6}^* phase has a biaxial six-layer structure with a long helical pitch. Here $Q_o = 2\pi/d$. The resonant nature of the split peaks is highlighted by the disappearance of the satellite peaks in the data obtained from an x-ray energy slightly off (by $0.011keV$) the resonant energy ($Eo = 2.471keV$). On the basis of symmetry

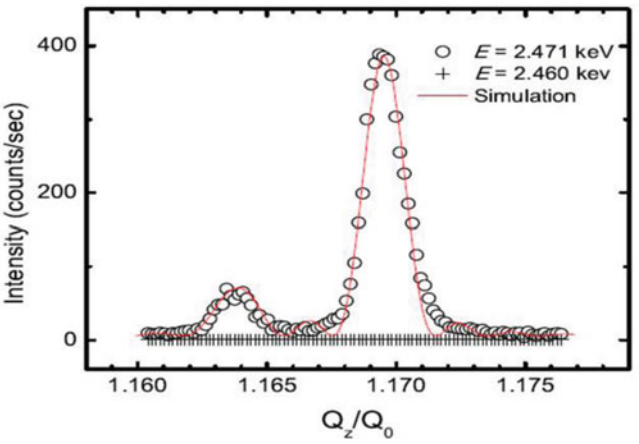

Figure 6. The resonant satellite peak (circles) from *mixture A* at 80.89°C and the simulation (line). Crosses are off-resonance data obtained at E = 2.460 *keV*. The center of the split peaks is located at $Q_z/Q_0 = 1.167$, corresponding to a pitch of six layers. The split peaks indicate a distorted helical structure. The positions and intensities of the two peaks give an optical pitch of 350 layers (1.36 μm) and a distortion angle δ_6 of (27± 2)°. The simulation has been normalized to match the measured intensities. The structure used in our fitting is given in Fig. 1.

arguments, Osipov and Gorkunov [17] have discussed this structure. By employing Levelut and Pansu's calculation of the tensor x-ray structure factor (T-SF) [7], detailed numeric simulations have been carried out. Two limiting cases characterized by special values of the distortion angle (δ_6) are the following: (a) for the planar structure ($\delta_6 = 0$), two peaks have equal intensities. The separation of the peaks is inversely related to the magnitude of the long helical pitch; (b) for the uniaxial structure ($\delta_6 = 60°$), there will be only one peak. The definition of δ_6 is given in Fig. 1. Consequently, the split peaks with different intensities indicate unambiguously that this $SmC_{d6}{}^*$ phase has a distorted helical structure. The solid curve in Fig. 6 shows a fit of the T-SF to the data with $\delta_6 = 27° \pm 2°$ and a long optical pitch of 350 layers (about 1.36 μm). Over the small temperature windows of the $SmC_{d6}{}^*$ phase from both mixtures, the distortion angles show only a small variation with temperature.

In addition to the $SmC_{d6}{}^*$ phase, a mysterious noisy region (N.R.) was found between the $SmC_{d6}{}^*$ and $SmC_{d4}{}^*$ phases in both *mixture A* and *B*. Extensive RXRD investigations were later conducted on *mixture B* [18]. A representative RXRD scan acquired at T = 76.81°C is shown in Fig. 7 over a wide range of Q_z ($1.13 < Q_z/Q_o < 1.25$). In order to reveal the resonant nature of the features, data obtained from an off-resonant scan are shown. For comparison, the figure also includes the sharp resonant peak from the $SmC_{d6}{}^*$ phase (at T = 78.35°C). Note different vertical scales are used. The tail of the principal Bragg peak at $Q_z/Q_o = 1.00$ is clearly visible. Upon subtracting the non-resonant contribution, the resonant part of the data can readily be obtained within this window of Q_z/Q_o. Within the noisy region (75.6°C < T < 77.5°C), resonant data were acquired with 30 mK/step cooling runs. The resulting resonant spectra are compiled as an intensity contour plot. To account for the beam damage and chemical degradation of the film, all the scans are normalized according to the integrated intensities of their corresponding principal Bragg peaks. Thus the contours of the resonant intensities related to orientational structures of the sample as a function of temperature and Q_z/Q_o are obtained [18]. The major features are summarized

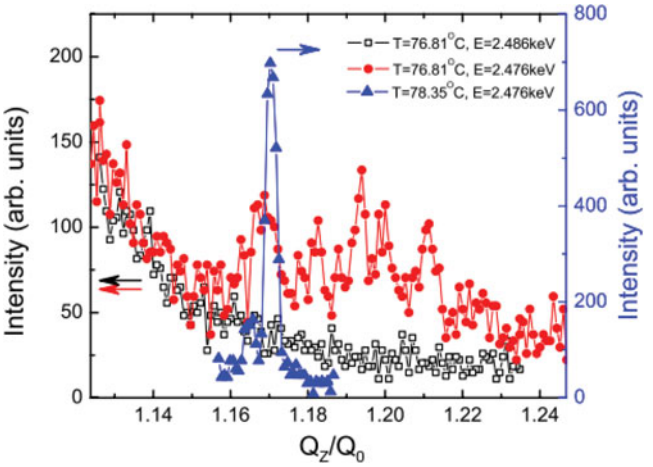

Figure 7. Representative data of the RXRD experiments from *mixture B*. Resonant scans in the noisy region (red dots, T = 76.81°C) and the SmC_{d6}^* phase (blue triangles, T = 78.35°C) as well as off-resonant scan in the noisy region (black squares) are shown as a function of Q_Z/Q_0. Note the SmC_{d6}^* data are shown on a different intensity scale (right axis) (from Ref. [18]).

as follows. First, upon cooling multiple and random resonant peaks are visible across the noisy region, while the center of those peaks gradually and consistently shifts toward higher Q_z values. Second, the resonant peaks observed in the noisy region are all contained in the Q_z-value ranging from around $Q_z/Q_o = 1.16$ up to about $Q_z/Q_o = 1.24$. There exists a gradual evolution of the main features of the resonant signals. From various experimental runs employing different rates of heating and cooling through the noisy region, both the noisy feature of the resonant data and the temperature window remain unchanged. Thus we conclude that the noisy region is thermodynamically stable.

Related Work

Soon after our discovery of the SmC_{d6}^* phase being published, A. D. L. Chandani *et al.* [19] studied binary mixtures of $(10OHF)_{(1-x)}(C11)_x$ with concentrations (x = 0.1105 and 0.1148) similar to our *mixture B*. The liquid crystal mixtures were placed in 25 μm-thick homeotropic sample cells. Upon applying an in-plane electric field to the samples, a photo-elastic modulator was utilized to measure electric-field induced birefringence as a function of temperature. Constant birefringence contours are plotted in the electric field versus temperature graphs in Fig. 8. From the changes in birefringence contours, various phase transitions were mapped out. Upon cooling, the following phase sequence was proposed: SmC_α^*- SmC_{d6}^*-SmC_{d5}^*-SmC_{d4}^* -SmC^* for both mixtures [19]. Later, another three mixtures (x = 0.1245, 0.1350, and 0.1500) were investigated [20] by the same research group using the same experimental probe. An identical phase sequence was reported. The most distinct difference between the results from RXRD and electric-field induced birefringence is that the noisy region found in the RXRD is replaced by the SmC_{d5}^* phase which shows a 5-layer periodicity. During our synchrotron run of investigating the noisy region in *mixture B* ($(10OHF)_{(1-x)}(C11)_x$ with x = 0.11), we paid special attention to the region near $Q_z/Q_o = 1.20$ and made sure that the mesophase having a 5-layer periodicity was not overlooked. There existed no trace of a resonant signal near $Q_z/Q_o = 1.20$ at all. For

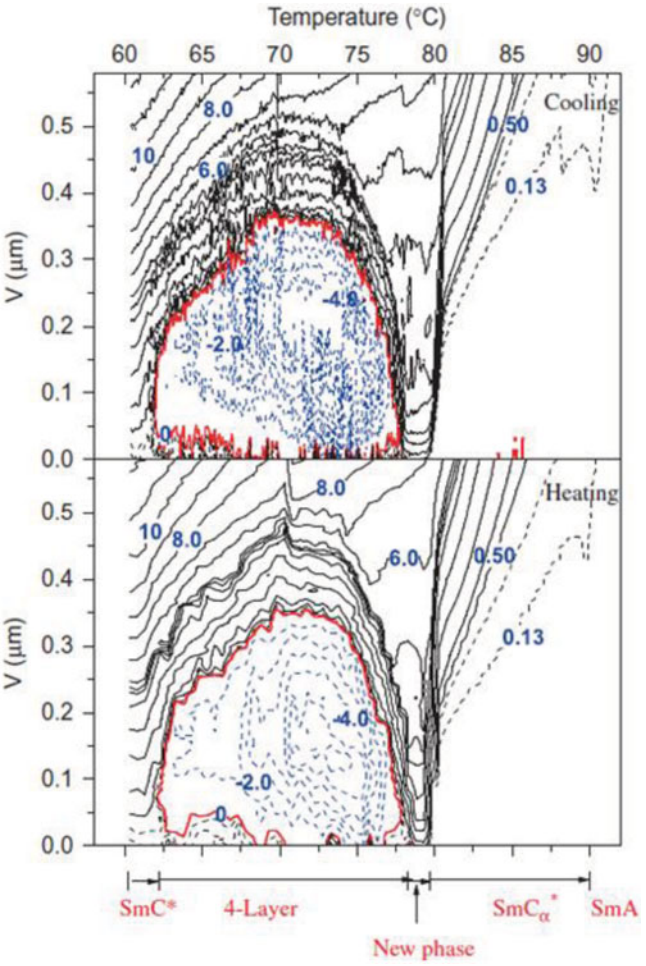

Figure 8. V-T phase diagrams for the binary mixture $(10OHF)_{0.8895}$ $C11_{0.1105}$ upon cooling and heating. The contours are at intervals $\Delta n = 1 \times 10^{-3}$. The red line represents $\Delta n = 0$. The phase sequence are the following: SmA(90.4°C)SmC_α*(79.7°C) new phase (77.9°C) SmC_{d4}*(61.7°C) SmC* (cooling) and SmC*(61.8°C) SmC_{d4}*(78.8°C) new phase (79.8°C) SmC_α*(90.3°C) SmA (from Ref. [20]).

this reason, we decided to carry out detailed analyses of the noisy contours applying both a percolation model and a nucleation model of co-existing SmC_{d4}* and SmC_{d6}* regions. The simulation results from the percolation model reproduced the observed noise contours significantly better than those from the nucleation model [18]. Hence, our detailed RXRD data do not support the existence of the SmC_{d5}* phase hypothesized to explain the reported electric-field-induced birefringence data.

Recently, Y. Takanishi *et al.* [11] have obtained dielectric responses and two-dimensional microbeam RXRD profiles as a function of temperature from one binary mixture ($A_{0.9}B_{0.1}$). The compound A contains a Br atom in the core part of the molecule. By tuning the incident x-ray energy to the bromine K absorption edge (13.48 *keV*), the resultant RXRD data yield orientational satellite spots. As temperature increases, satellite

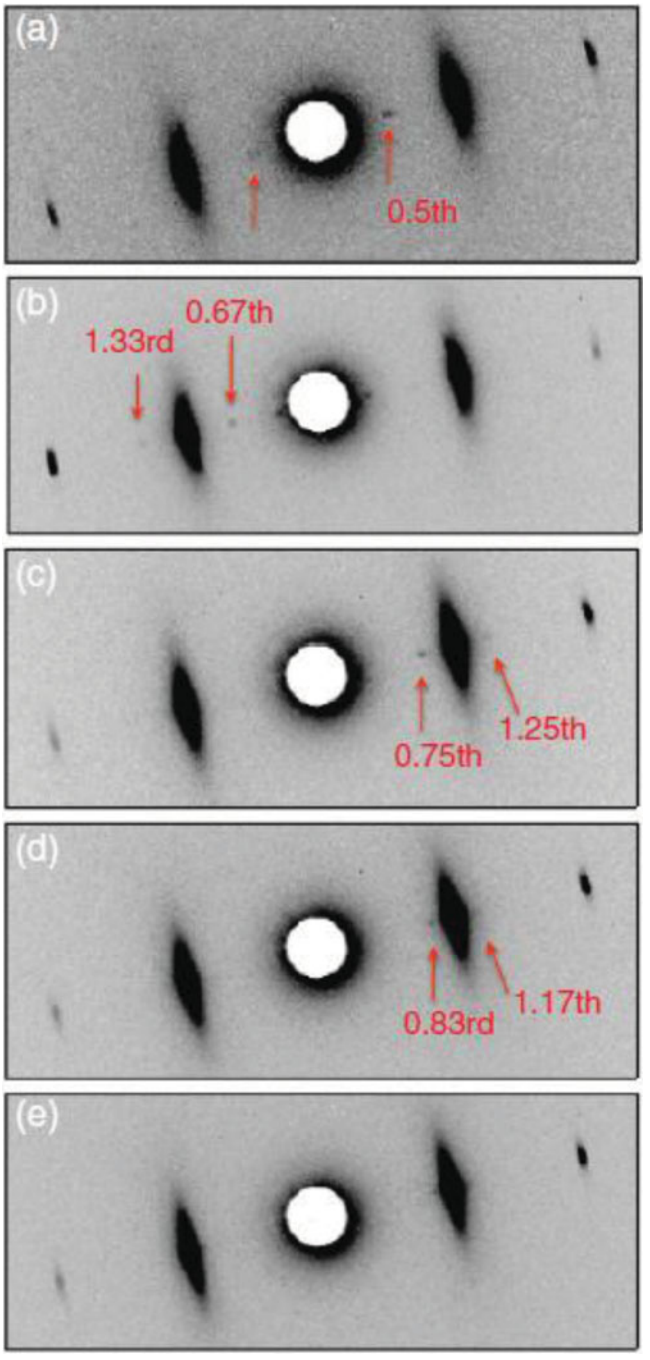

Figure 9. Two-dimensional microbeam RXRD profiles at five selected temperatures: (a) 105°C, (b) 111°C, (c) 118°C, (d) 121°C, and (e) 124°C. Red arrows point to the satellite peaks (from Ref. [21]).

spots corresponding to 2-, 3-, 4-, 6- layer structures are visible from a two-dimensional pixel array detector (Fig. 9). The resolution of the detector is not high enough to resolve the details of the satellite peaks. The mesophase having a six-layer structure ($Q_z/Q_o = 0.83$ or 1.17) produced a ferrielectric-like dielectric response over about 3K temperature range. Consequently, Y. Takanishi *et al*. assigned the phase to be $SmC_A^*(q_T = 2/3)$. High-resolution polarization-analyzed RXRD studies [21] should yield additional information of this phase. There are two critical differences between the two mesophases (SmC_{d6}^* and SmC_A^* ($q_T = 2/3$)) with a six-layer structure. First, the SmC_{d6}^* structure shows antiferroelectric-like optical responses while the $SmC_A^*(q_T = 2/3)$ structure exhibits ferrielectric-like dielectric responses. Secondly, the phase transition sequences involved are very different. In light of the different structures of these two six-layer mesophases along with several theoretically proposed structures, L. D. Pan *et al.* [22] carried out extensive computer simulations of the different possible models of interlayer ordering showing the resonant spectra that would result for the different possible structures of a smectic C^* phase with a six-layer periodicity. These calculated polarization-resolved resonant spectra should guide future measurements since they highlight the distinctive resonant spectral features associated with the different possible structures.

Summary

In 1982, our research group reported calorimetric data on the SmA-SmC transition of racemic 2M4P9OBC [4-(2'-methylbutyl)phenyl 4-n-nonyloxybiphenyl-4-carboxylate] and revealed that this heat capacity can be well described by an extended mean-field model [23]. Subsequently, many research groups have confirmed the mean-field behavior in various liquid crystal compounds/mixtures showing the SmA-SmC or SmA-SmC* transitions [24-31]. Because the symmetry of the order parameter associated with the SmA-SmC transition is XY-like [1, 2]. Consequently, the only possible source of this mean-field behavior is long range interactions. Here the mesophases with six-layer periodicity have been found in two very different liquid crystal systems. Moreover, our recent null-transmission ellipsometry investigations of surface-surface interaction from free-standing films of MHPBC [4-(1-methylheptoloxycarbonyl)phenyl 4′-octylbiphenyl-4-carboxylate] yield quasi-long range interactions between two surface layers [32]. The smectic phases (i.e., SmA, SmC, SmC_α^*, SmC*, SmC_{d6}^*, SmC_{d4}^*, SmC_{d3}^*, and SmC_A^*) reported here have two-dimensional in-plane liquid-like order. Intuitively, short-ranged interlayer interactions are expected. Thus "What is the origin of the observed long-range or quasi-long-range interlayer interactions?" [33] is a fundamental question of condensed matter physics.

References

[1] de Gennes, P. G., & Prost J. (1998). *The Physics of Liquid Crystals, second edition*, Clarendon, Oxford.
[2] Chandrasekhar, S. (1992). *Liquid Crystals, second edition*, Cambridge University Press, Cambridge.
[3] Takezoe, H., Gorecka, E., & Cepic, M. (2010). *Rev. Mod. Phys.*, *82*, 897.
[4] Laux, V., Isaert, N., Faye, V., & Nguyen, H. T. (2000). *Liq. Cryst.*, *27*, 81.
[5] Wang, S. T., Liu, Z. Q., McCoy, B. K., Pindak, R., Caliebe, W., Nguyen, H. T., & Huang, C. C. (2006). *Phys. Rev. Lett.*, *96*, 097801.
[6] Sandhya, K. L., Song, J. K., Panarin, Yu. P., Vij, J. K., & Kumar, S. (2008). *Phys. Rev. E*, *77*, 051707.
[7] Levelut, A.-M., & Pansu, B. (1999). *Phys. Rev. E*, *60*, 6803.

[8] Mach, P., Pindak, R., Levelut, A. M., Barois, P., Nguyen, H. T., Huang, C. C., & Furenlid, L., (1998). *Phys. Rev. Lett.*, *81*, 1015.
[9] Matkin, L. S., Gleeson, H. F., Mach, P., Huang, C. C., Pindak, R., Srajer, G., Pollmann, J., Goodby, J. W., Hird, M., & Seed, A. (2000). *Appl. Phys. Lett.*, *76*, 1863.
[10] Cluzeau, P., Gisse, P., Ravaine, V., Levelut, A.-M., Barois, P., Huang, C. C., Rieutord, F., & Nguyen, H. T. (2000). *Ferroelectrics*, *244*, 1
[11] Takanishi, Y., Nishiyama, I., Yamamoto, J., Ohtsuka, Y., & Iida, A. (2013). *Phys. Rev. E*, *87*, 050503 (R).
[12] Cady, A., Pitney, J. A., Pindak, R., Matkin, L. S., Watson, S. J., Gleeson, H. F., Cluzeau, P., Barois, P., Levelut, A.-M., Caliebe, W., Goodby, J. W., Hird, M., & Huang, C. C. (2001). *Phys. Rev. E*, *64*, 050702(R).
[13] Wang, Shun, Pan, LiDong, McCoy, B. K., Wang, S. T., Pindak, R., Nguyen, H. T., & Huang, C. C. (2009). *Phys. Rev. E*, *79*, 021706.
[14] Schlauf, D., Bahr, Ch., & Nguyen, H. T. (1999). *Phys. Rev. E*, *80*, 6818.
[15] Johnson, P.M., Pankratz, S., Mach, P., Nguyen, H. T., & Huang, C. C. (1999). *Phys. Rev. Lett.*, *83*, 4073.
[16] Wang, Shun, Pan, LiDong, Pindak, R., Liu, Z.Q., Nguyen, H. T., & Huang, C. C. (2010). *Phys. Rev. Lett.*, *104*, 027801.
[17] Osipov M. A., & Gorkunov, M. V. (2006). *Liq. Cryst.*, *33*, 1133.
[18] Pan, LiDong, Barois, P., Pindak, R., Liu, Z. Q., McCoy, B. K., & Huang, C. C. (2012). *Phys. Rev. Lett*., *108*, 037801.
[19] Chandani, A. D. L., Fukuda, A., Kumar, S., & Vij, J. K. (2011). *Liq. Cryst.*, *38*, 663.
[20] Sandhya, K. L., Chandani, A. D. L., Fukuda, A., Kumar, S., & Vij, J. K. (2013). *Phys. Rev. E*, *87*, 062506.
[21] Mach, P., Pindak, R., Levelut, A.-M., Barois, P., Nguyen, H. T., Baltes, H., Hird, M., Toyne, K., Seed, A., Goodby, J. W., Huang, C. C., & Furenlid, L. (1999). *Phys. Rev. E.*, *60*, 6793.
[22] Pan, LiDong, Pindak, R., & Huang, C. C. (2014). *Phys. Rev. E*, *89*, 022501.
[23] Huang, C. C., & Viner, J. M. (1982). *Phys. Rev. A*, *25*, 3385.
[24] Birgeneau, R. J., Garland, C. W., Kortan, A. R., Litster, J. D., Meichle, M., Ocko, B. M., Rosenblatt, C., Yu, L. J., & Goodby, J. (1983). *Phys. Rev. A*, *27*, 1251.
[25] Meichle, M., & Garland, C. W. (1983). *Phys. Rev. A*, *27*, 2624.
[26] Dumrongrattana, S., & Huang, C. C. (1986). *Phys. Rev. Lett.*, *56*, 464.
[27] Liu, H. Y., Huang, C. C., Bahr, Ch., & Heppke, G. (1988). *Phys. Rev. Lett.*, *61*, 345.
[28] Seppen, A., Musevic, I., Maret, G., Zeks, B., Wyder, P., & Blinc, R. (1988). *J. Phys. France*, *49*, 1569.
[29] Boerio-Goates, J., Garland, C. W., & Shashidhar, R. (1990). *Phys. Rev. A*, *41*, 3192.
[30] Bahr, Ch., & Heppke, G. (1990). *Phys. Rev. Lett.*, *65*, 3297.
[31] Yang, F., Bradberry, G. W., & Sambles, J. R. (1994). *Phys. Rev. E*, *50*, 2834.
[32] Pan, LiDong, Hsu, C.S., & Huang, C.C. (2012). *Phys. Rev. Lett*., *108*, 027801.
[33] Hamaneh, M. B., & Taylor, P. L. (2005) *Phys. Rev. E*, *72*, 021706.